Dual-isotope 111In/177Lu SPECT imaging as a tool in molecular imaging tracer design

CONTRAST MEDIA & MOLECULAR IMAGING

Received: 28 June 2011, Revised: 10 August 2011, Accepted: 19 September 2011, Published online in Wiley Online Library: 2012

(wileyonlinelibrary.com) DOI: 10.1002/cmmi.485

Dual-isotope ^{111}In/^{177}Lu SPECT imaging as a tool in molecular imaging tracer design

Nicole M Hijnen[a], Anke de Vries[a], Klaas Nicolay[a] and Holger Grüll[a,b]*

The synthesis, design and subsequent pre-clinical testing of new molecular imaging tracers are topic of extensive research in healthcare. Quantitative dual-isotope SPECT imaging is proposed here as a tool in the design and validation of such tracers, as it can be used to quantify and compare the biodistribution of a specific ligand and its nonspecific control ligand, labeled with two different radionuclides, in the same animal. Since the biodistribution results are not blurred by experimental or physiological inter-animal variations, this approach allows determination of the ligand's net targeting effect. However, dual-isotope quantification is complicated by crosstalk between the two radionuclides used and the radionuclides should not influence the biodistribution of the tracer. Here, we developed a quantitative dual-isotope SPECT protocol using combined ^{111}Indium and ^{177}Lutetium and tested this tool for a well-known angiogenesis-specific ligand (cRGD peptide) in comparison to a potential nonspecific control (cRAD peptide). Dual-isotope SPECT imaging of the peptides showed a similar organ and tumor uptake to single-isotope studies (cRGDfK–DOTA, 1.5 ± 0.8%ID cm^{-3}; cRADfK–DOTA, 0.2 ± 0.1%ID cm^{-3}), but with higher statistical relevance (p-value 0.007, $n = 8$). This demonstrated that, for the same relevance, seven animals were required in case of a single-isotope test design as compared with only three animals when a dual-isotope test was used. Interchanging radionuclides did not influence the biodistribution of the peptides. Dual-isotope SPECT after simultaneous injection of ^{111}In and ^{177}Lu-labeled cRGD and cRAD was shown to be a valuable method for paired testing of the *in vivo* target specificity of ligands in molecular imaging tracer design.
Supporting information may be found in the online version of this paper.

Keywords: tracer design; targeting; dual-isotope SPECT; molecular imaging; cRGD; cRAD; crosstalk

1. INTRODUCTION

Molecular imaging aims at earlier and more specific detection of diseases by imaging disease-related molecular and cellular processes that precede morphological changes. Key are molecular imaging tracers that specifically home in on disease-related molecular markers and render them detectable with one of the diagnostic imaging techniques. Consequently, synthesis and design of new molecular imaging tracers, their subsequent pre-clinical testing and clinical validation are topics of extensive research (1).

Disease-related markers typically have expression levels in the picomolar to nanomolar range, leading to similar concentrations of bound imaging agents (2). Therefore, sensitive optical techniques or nuclear modalities like positron emission tomography (PET) and single photon emission computed tomography (SPECT) seem to be the most suited for molecular imaging as they allow detection of tracers in the picomolar to nanomolar range (2). While PET imaging is currently more sensitive than SPECT and superior in quantification, SPECT has an advantage over PET when it comes to simultaneous imaging of two different radionuclides, i.e. dual-isotope imaging. The cameras used in SPECT scanners are equipped with energy-resolved detectors that can distinguish between different γ-emitting radionuclides based on their differences in emission energies. Simultaneous detection of multiple probes with different spectral characteristics is also possible with optical imaging; however, it is limited to more superficial malignancies owing to the penetration depth of light photons.

Although there are several clinical examples of dual-isotope SPECT in cardiac imaging (3), brain imaging (4) and osteomyelitis (5,6), broad clinical adoption is still lacking. In pre-clinical research, a dual-isotope approach recently showed its value for investigation of organ function (7) or unraveling biological mechanisms, for example the activation of peptide-based molecular imaging probes *in vivo* (8). We expect quantitative dual-isotope imaging to also hold great potential as a tool in the design and validation of new molecular imaging tracers, since it can be used to quantify and compare the biodistribution of a specific ligand and its nonspecific control ligand, labeled with two different γ-emitting radionuclides, simultaneously in the same animal. Here, we present a dual-isotope imaging approach that enables the investigation of the net uptake of a tracer by eliminating any inter-animal differences and physiological changes (Fig. 1a). This paired design leads to fewer degrees of freedom compared with the usually performed unpaired testing and therefore to a decrease in the number of animals that are required to obtain a statistically relevant result.

One of the reasons why broad clinical application of dual-isotope SPECT is lacking is the challenge of obtaining

* *Correspondence to: Department of Bio-molecular Engineering, Philips Research Eindhoven, The Netherlands; Department of Biomedical Engineering, Eindhoven University of Technology, The Netherlands.*
E-mail: holger.gruell@philips.com; h.gruell@tue.nl

a *N. M. Hijnen, A. Vries, K. Nicolay, H. Grüll*
Biomedical NMR, Department of Biomedical Engineering, Eindhoven University of Technology, The Netherlands

b *H. Grüll*
Department of Bio-molecular Engineering, Philips Research Eindhoven, The Netherlands

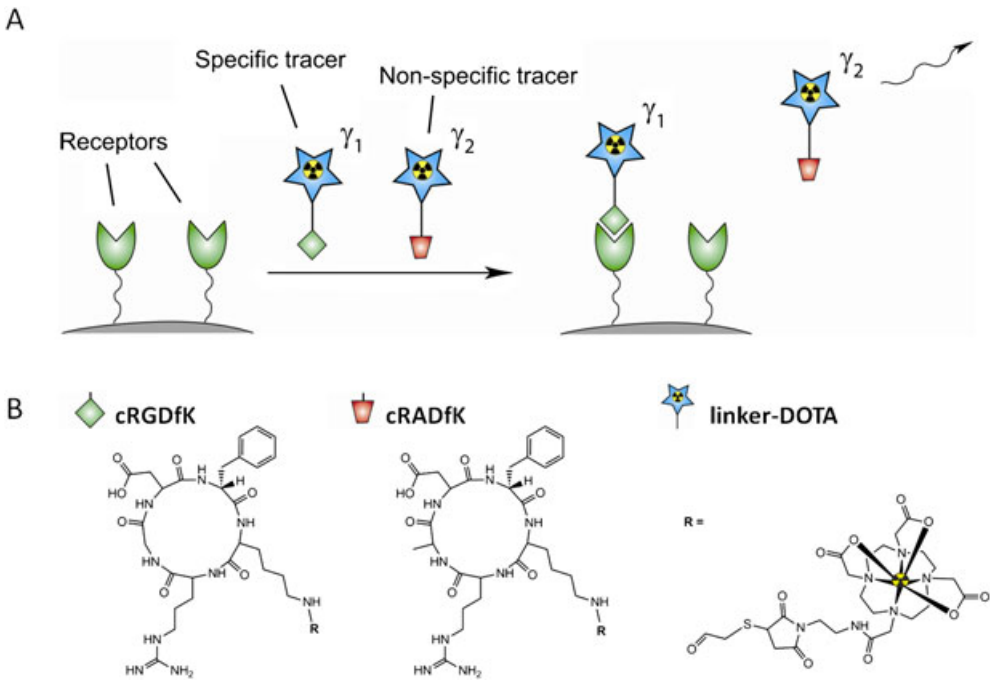

Figure 1. (a) Specific and nonspecific tracer simultaneously in one animal, to be imaged with dual-isotope SPECT and (b) structural formulas of the probes used. ^{111}In and ^{177}Lu were used as radiolabel in this study.

quantitative information from dual-isotope SPECT scans (9,10). Overlap in the emission spectra of the two respective radionuclides as well as Compton scattering result in crosstalk between the signals coming from these radionuclides. Crosstalk is defined as the detection of photons originating from one radionuclide in the acquisition window of the other, and results in artifacts and quantification errors (9,11). Therefore, quantitative dual-isotope imaging requires the development of new protocols as compared with conventional single-isotope imaging to compensate for crosstalk effects. Examples of such methods include the use of additional energy windows that allow quantification of the extent of the crosstalk followed by subtraction or model-based methods (9,12). Another approach is to minimize crosstalk effects by re-positioning the acquisition energy window and careful choice of the radionuclide combination used. To date, the radionuclide combinations that are used most often for dual-isotope imaging include combined ^{123}I/^{99m}Tc (4), ^{201}Tl/^{99m}Tc (13), ^{131}I/^{99m}Tc (14) and ^{111}In/^{99m}Tc (15). However, for the purpose of comparing the biodistribution of a specific ligand directly with its nonspecific control, the choice of radionuclides is restricted since both radionuclides have to be suited to radiolabeling the ligands via the same chelator. The latter is of great importance since the chelator itself could change the biodistribution of the tracer, thereby hindering direct comparison of the ligands. Herein, the DOTA chelator (1,4,7,10-tetraazacyclododecane-*N*,*N*′,*N*″,*N*‴ tetraacetic acid) is the preferred choice since its macrocyclic structure in general forms more stable chelates than the DTPA chelator (diethylene triamine pentaacetic acid) (16). Furthermore, the radionuclide itself should not have a different effect on the biodistribution, or influence the binding affinity of the ligands. Finally, the radionuclides require half-lives that is similar to each other and suitable for the study duration. These requirements led us to choose ^{111}In and ^{177}Lu as a radionuclide couple, although we are aware that ^{177}Lu is not ideal for use in diagnostic clinical imaging studies owing to its β emission.

In this work, we developed and optimized a quantitative ^{111}In/^{177}Lu dual-isotope SPECT imaging protocol to establish it as a tool in pre-clinical tracer design. For this methodological study, we decided to use the well-characterized angiogenesis-specific ligand cyclic arginine–glycine–aspartate peptide (cRGD) (17) in direct comparison to cyclic arginine–alanine–aspartate peptide (cRAD) that serves as the internal control. The cRGD peptide is known to have a high affinity for the $\alpha_v\beta_3$ cell surface integrin, which is overexpressed on specific tumor cells and endothelial cells in angiogenic blood vessels (18–24). In cRAD, the glycine residue is changed into alanine, and it is suggested that with this mutation the affinity for $\alpha_v\beta_3$-integrin is lost (Fig. 1b) (25,26). As a proof of concept, we carried out a dual-isotope SPECT study to investigate how this minor difference in chemical structure translates into loss of specificity and potential changes in the biodistribution. As dual isotope allows the direct comparison in the same animal, we expect to arrive at statistical relevant data with fewer animals compared with the classical approach using an unpaired study design.

2. RESULTS AND DISCUSSION

The ^{111}In/^{177}Lu couple was chosen for dual-isotope imaging based on their radiochemical and physical characteristics. Both radionuclides have a half-life suitable for the study duration, and allow radiolabeling of a ligand via a DOTA chelator. Furthermore, these radionuclides have minimal overlap in the γ-emission energy spectra (Supporting Information, table 1). The ^{177}Lu radionuclide is, besides a γ-emitter, also a β-emitter used for therapy. Therefore, the ^{111}In/^{177}Lu radionuclide combination is primarily suitable for use in short-term pre-clinical biodistribution studies where possible radiotoxic effects are not of major importance, although short-term effects on the uptake of other tracers cannot be fully excluded (27).

Table 1. Phantom and *in vivo* crosstalk factors (cc-factor) from γ_1 to γ_2 ($\gamma_1 \rightarrow \gamma_2$) and vice versa as measured on the SPECT/CT

Setting[a]	Phantom cc-factor $^{177}Lu \rightarrow {}^{111}In$	Phantom cc-factor $^{111}In \rightarrow {}^{177}Lu$	*In vivo* cc-factor $^{177}Lu \rightarrow {}^{111}In$	*In vivo* cc-factor $^{111}In \rightarrow {}^{177}Lu$
1	0.0682 ± 0.0004[b]	0.1489 ± 0.0003[b]	0.1253 ± 0.0134[b]	0.2034 ± 0.0022[b]
2	0.0913 ± 0.0009[b]	0.0273 ± 0.0002[b]	0.1798 ± 0.0220[b]	0.0400 ± 0.0003[b]

[a]The acquisition energy windows settings corresponding to setting 1 and 2 are stated in the text.
[b]Measured in triplicate using static planar scans, acquiring >100 kcounts per projection (mean value ± SD).
[c]Measured in BALB/c nu/nu mice (average weight 24 g).

2.1. Dual-isotope optimalization

To allow for quantitative $^{111}In/^{177}Lu$ SPECT imaging, the acquisition settings were optimized to minimize the amount of crosstalk by adjusting the acquisition energy windows settings. Optimizing the acquisition settings to three 10% energy windows around 171, 208 and 245 keV resulted in a reduction of the mean error on ^{111}In-quantification of 3.6 into 2.9% and for ^{177}Lu-quantification from 38.0 13.9% error in phantoms (Fig. 2a).

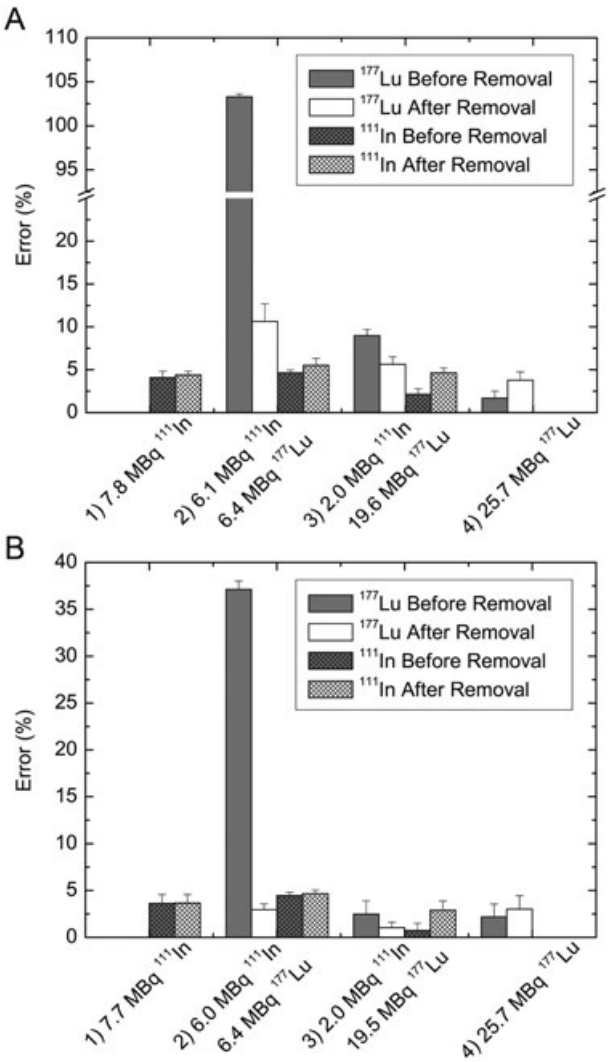

Figure 2. Quantification error percentages for dual-isotope $^{111}In/^{177}Lu$ SPECT imaging in phantoms using (a) energy window setting 1 and (b) energy window setting 2.

Crosstalk from ^{111}In to ^{177}Lu was more severe than vice versa. Part of the remaining crosstalk could be removed by using a subtraction-based software correction method that made use of a crosstalk calibration factor. After the software correction, the mean error on ^{111}In-quantification in phantoms increased slightly from 2.9 to 3.6%, while the mean error on ^{177}Lu-quantification reduced from 13.9 to 2.3% (Fig. 2b).

The dual-isotope protocol was tested in an *in vivo* experiment by studying the biodistribution of the free radionuclides with both single- and dual-isotope acquisition (Fig. 3). The biodistribution of both radionuclides determined with single-isotope SPECT studies corresponded to earlier results reported in literature. In fact, noncarrier-added (n.c.a.) ^{111}In is known to bind to transferrin and other proteins in blood (28) leading to an uptake in liver, while the remaining ^{111}In is eliminated by the kidneys. N.c.a. ^{177}Lu acts as calcium mimic *in vivo* and accumulates in bone (29). A comparable biodistribution was found for simultaneous injection of both isotopes using dual-isotope SPECT studies and applying crosstalk removal, with no significant ^{111}In related activity detected in the bones, and no significant ^{177}Lu related activity in the kidneys and liver (Fig. 3a, b). A linear correlation was found between the biodistribution quantified from single- and dual-isotope SPECT studies (^{111}In, $R^2 \approx 0.94$; and ^{177}Lu, $R^2 \approx 0.92$, Supporting Information, figure 4; Fig. 3c), supporting the use of dual-isotope $^{111}In/^{177}Lu$ SPECT for *in vivo* quantification.

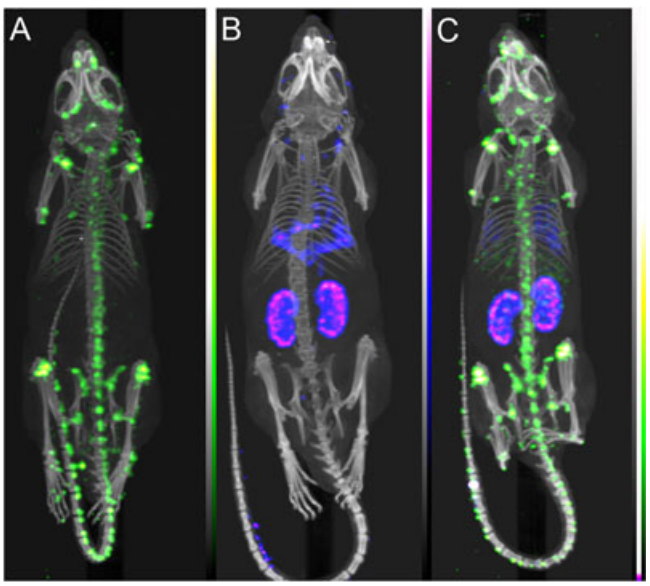

Figure 3. SPECT/CT images of single-isotope acquisition of (a) ^{177}Lu (green), (b) ^{111}In (blue/purple) and (c) dual-isotope simultaneous acquisition of ^{177}Lu (green) and ^{111}In (blue/purple) (all 3 h circulation time).

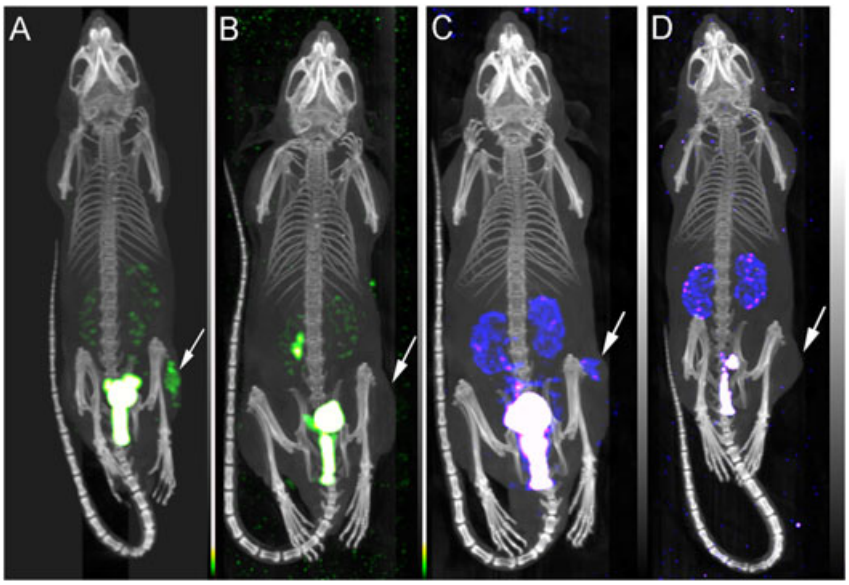

Figure 4. Combined SPECT/CT images of tumor bearing mice 1 h after injection of (a) 1.32 nmol ^{177}Lu–DOTA–cRGDfK, (b) 1.32 nmol ^{177}Lu–DOTA–cRADfK, (c) 1.32 nmol ^{111}In–DOTA–cRGD and (d) 1.32 nmol ^{111}In–DOTA–cRADfK. The white arrows point to the tumor locations.

2.2. Single-isotope

Single-isotope studies showed specific tumor uptake of ^{177}Lu–DOTA–cRGDfK (0.97 ± 0.19%ID cm^{-3}, Fig. 4a). Most of the injected peptide was eliminated through the urinary system, as confirmed by the presence of high activity in the bladder and some residual activity in the kidneys. No ^{177}Lu activity was found in bone, suggesting tracer stability *in vivo*. The highest tumor uptake was found after injection of low amounts of cRGD (γ-counting: 6.5 ± 1.9%ID g^{-1} after injection of 0.26 nmol peptide instead of 1.32 nmol peptide). This finding was in line with previous research in which saturation of the $\alpha_v\beta_3$-receptors was reported to occur at RGD peptide doses >0.26 nmol (30), resulting in lower uptake percentages of the injected dose and increased nonspecific uptake in the intestines. However, to obtain a sufficiently high activity for SPECT imaging using ^{111}In as radiolabel, a minimum peptide dose of 1.32 nmol was required. For exact comparison the same amount of peptide dose should be used for both the specific tracer and the nonspecific control. Therefore, 1.32 nmol of each peptide was used during further experiments for both radiolabels, unless otherwise stated.

A similar biodistribution was found with SPECT and γ-counting (linear correlation, $R^2 \approx 0.74$), although quantification of the tissue-uptake from SPECT data consistently resulted in lower uptake percentages than quantification using γ-counting (2.41 ± 0.56%ID g^{-1} tumor uptake using γ-counting compared with 0.97 ± 0.19%ID cm^{-3} using SPECT, Fig. 5). Apart from the differences in tissue density that are present in the %ID cm^{-3} (SPECT) compared with the%ID g^{-1} (γ-counter) data, this difference was caused by the method of volume of interest (VOI) selection during SPECT analysis. In this method a cylindrical volume was drawn around the tissue of interest, causing an overestimation of the tissue volume, which translates to an underestimation in %ID cm^{-3}.

After injection of ^{177}Lu–DOTA–cRADfK, no significant tumor uptake was found with both SPECT (0.00 ± 0.00%ID cm^{-3}) and γ-counting (0.26 ± 0.01%ID g^{-1}; Figs 4b and 5). Apart from the tumor tissue, the biodistribution of ^{177}Lu–DOTA–cRADfK was similar to that of ^{177}Lu–DOTA–cRGDfK. The above experiments were repeated for DOTA–cRGDfK and DOTA–cRADfK labeled with ^{111}In instead of ^{177}Lu to assess the influence of the radionuclide on the tracer biodistribution. No difference in biodistribution was observed between ^{111}In- and ^{177}Lu- labeled peptides (Figs 4c, d and 5). As expected, tumor uptake was observed for ^{111}In–DOTA–cRGDfK (SPECT, 0.75 ± 0.14%ID cm^{-3}; γ-counting, 2.34 ± 2.09%ID g^{-1}), but not for ^{111}In–DOTA–cRADfK (SPECT, 0.08 ± 0.06%ID cm^{-3}; γ-counting, 0.41 ± 0.33%ID g^{-1}).

The difference in tumor uptake between radiolabeled DOTA–cRGDfK and DOTA–cRADfK was significant based on both the SPECT and γ-counter data separately (1.32 nmol peptide, $n = 8$, p-value ≈ 0.0209, Kruskal–Wallis test). Taking all single-isotope targeting studies together, an even higher significance was obtained (1.32 nmol and 0.26 nmol peptide, $n = 12$, p-value 0.0039, Kruskal–Wallis test).

2.3. Dual-isotope

For the dual-isotope study, five mice were co-injected with ^{177}Lu–DOTA–cRGDfK and ^{111}In–DOTA–cRADfK (Figs 6a and 7a). The mice were imaged using the energy windows of setting 2 (10% windows around 171, 208 and 245 keV) and crosstalk was removed. The ^{177}Lu-frame showed tumor uptake of the ^{177}Lu–DOTA–cRGDfK, while no tumor uptake of ^{111}In–DOTA–cRADfK was visible in the ^{111}In-frame. The biodistribution for both tracers was similar to the biodistribution found during single-isotope studies with 1.32 nmol peptide. Tumor uptake of cRGD (SPECT: 1.54 ± 0.92%ID cm^{-3}, γ-counting: 3.40 ± 0.47%ID g^{-1}) and cRAD (SPECT: 0.17 ± 0.08%ID cm^{-3}, γ-counting: 0.18 ± 0.13%ID g^{-1}) was comparable with the tumor uptake found in single-isotope studies (Tables 1 and 2). This indicated that co-injection of the tracers did not influence the accumulation of the specific tracer at the target, which is a pre-requisite for using the dual-isotope approach as suggested.

Subsequently, four mice were co-injected with ^{111}In–DOTA–cRGDfK and ^{177}Lu–DOTA–cRADfK, in order to investigate any possible changes in biodistribution or binding affinity following radionuclide interchange [as was previously shown to be the

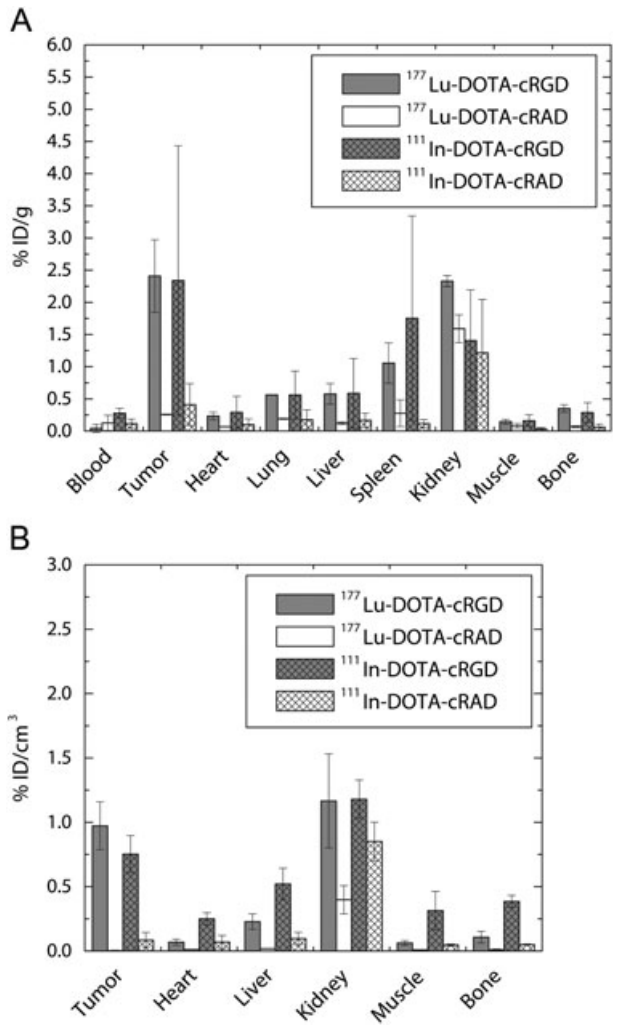

Figure 5. Biodistribution results 1 h after injection of 1.32 nmol ^{177}Lu–DOTA–cRGDfK ($n = 2$), 1.32 nmol ^{177}Lu–DOTA–cRADfK ($n = 2$), 1.32 nmol ^{111}In–DOTA–cRGDfK ($n = 2$) and 1.32 nmol ^{111}In–DOTA–cRADfK ($n = 2$) from (a) γ-counting (%ID g^{-1}) and (b) SPECT (%ID cm^{-3}).

case for DOTA-conjugated somatostatin analogs (31)]. The mice were imaged 1 h after injection using the same protocol as for the first group. SPECT dual-isotope showed tumor uptake of ^{111}In–DOTA–cRGDfK, while no tumor uptake could be visualized in the corresponding ^{177}Lu-frame (Fig. 6b). Apart from the tumor site, the biodistribution of both ligands was similar (Fig. 7b). The quantified tumor uptake corresponded to previous single- and dual-isotope studies (cRGD SPECT, 1.50 ± 0.72%ID cm^{-3}; cRGD γ-counting, 2.94 ± 0.31%ID g^{-1}; cRAD SPECT, 0.26 ± 0.05%ID cm^{-3}; cRAD γ-counting, 0.24 ± 0.13%ID g^{-1}; Table 2). Again quantification of the tissue uptake from SPECT data consistently resulted in lower uptake percentages than quantification using γ-counting. However, the strength of dual-isotope SPECT studies is that the same VOI can be used to quantify both the cRGD and cRAD biodistribution, eliminating this effect in direct comparison.

The difference in tumor uptake between radiolabeled DOTA–cRADfK and radiolabeled DOTA–cRGDfK was significant based on both the SPECT and γ-counter data from the dual-isotope studies (1.32 nmol peptide, $n = 9$, p-value: 0.0045, signed-rank test).

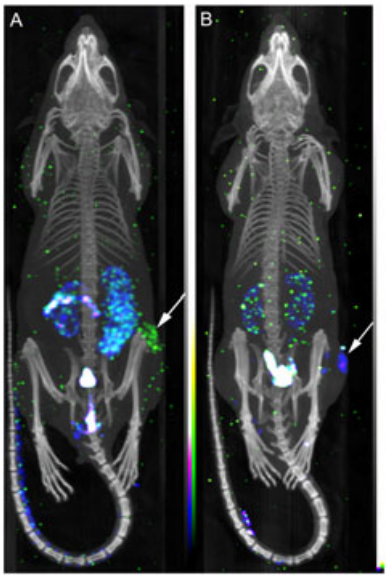

Figure 6. Dual-isotope SPECT/CT images of tumor bearing mice, 1 h post co-injection of (a) 1.32 nmol ^{177}Lu–DOTA–cRGDfK (yellow-green colormap) and 1.32 nmol ^{111}In–DOTA–cRADfK (blue-purple colormap) and (b) 1.32 nmol ^{111}In–DOTA–cRGDfK (blue-purple colormap) and 1.32 nmol ^{177}Lu–DOTA–cRADfK (yellow-green colormap). The white arrows point to the tumor locations.

As final control, two mice were co-injected with ^{177}Lu–DOTA–cRGDfK and ^{111}In–DOTA–cRGDfK. No significant difference between tumor uptake of both tracers was observed (^{177}Lu SPECT, 1.80 ± 0.44%ID cm^{-3}; ^{177}Lu γ-counting, 2.54 ± 0.91%ID g^{-1}; ^{111}In SPECT, 1.58 ± 0.41%ID cm^{-3}; ^{111}In γ-counting, 2.65 ± 1.21%ID g^{-1}; Table 2).

2.4. Statistics

There are fewer degrees of freedom when a pair of tracers is assessed in one animal, resulting in a statistical benefit requiring fewer experiments, and therefore fewer animals, to obtain a statistically relevant result. In Table 3, an approximation of this effect is illustrated for normally distributed data with equal variances, showing that, for the same statistical relevance, seven animals are required in case of an independent (single-isotope) test design, compared with three animals when a paired (dual-isotope) test design is used.

Ranked testing was performed to analyze our data because a normal distribution with equal variances could not be ensured owing to the limited sampling size [$n = 8$; Kruskal–Wallis test for single-isotope (unpaired) and the Signed-Rank test for dual-isotope (paired)]. Based on the single-isotope studies, a statistical relevant difference between tumor uptake of radiolabeled cRGD and cRAD was obtained with a p-value of 0.0209 in eight experiments. With the same amount of experiments in dual-isotope setting, a decrease in p-value was obtained to a p-value of 0.0071. The same statistical relevance was obtained for the single- and dual-isotope data quantified from SPECT imaging and γ-counting, showing that the difference in tissue-uptake percentages between the two methods does not influence the statistics when ranked testing is used. In this paper we show that, by using the dual-isotope approach, the number of animal studies required for quantification of the net-targeting effect of new molecular imaging tracers can be significantly reduced.

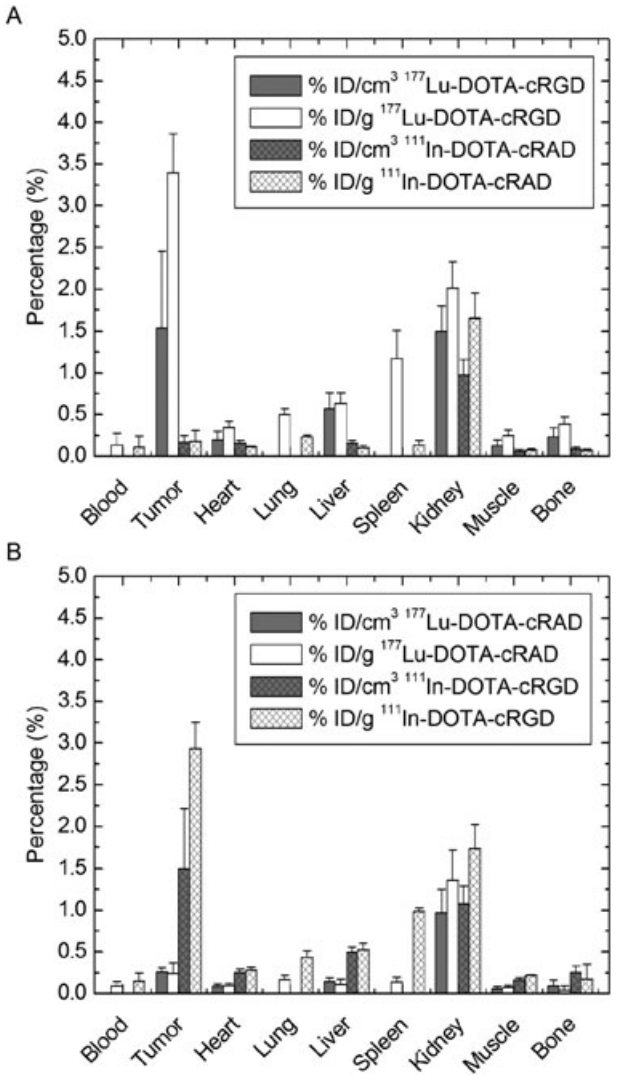

Figure 7. Biodistribution results 1 h post co-injection of (a) 1.32 nmol ^{177}Lu–DOTA–cRGDfK and 1.32 nmol ^{111}In–DOTA–cRADfK ($n = 5$) and (b) 1.32 nmol ^{177}Lu–DOTA–cRADfK and 1.32 nmol ^{111}In–DOTA–cRGDfK ($n = 4$) from SPECT (%ID cm^{-3}) and γ-counting (%ID g^{-1}).

Table 3. Statistical benefit of paired design testing[a]

Test design	Required sampling size (n)	Example
Independent	$n = \frac{2(z_\alpha + z_\beta)^2 s^2}{d^2}$ [b, c]	$n = \frac{2(1.65+1.28)^2 \cdot 0.6^2}{1^2} = 6.18$ [b]
Paired	$n = \frac{(z_\alpha + z_\beta)^2 s_d^2}{d^2}$ [b, c]	$n = \frac{(1.65+1.28)^2 \cdot 0.5^2}{1^2} = 2.15$ [b]

[a]For normally distributed data with equal variances. The formulas only give an approximation when a small sampling size is used (like in this example).
[b]n = sampling size/number of animals; z, z-statistic; α, significance level, for example 5%; $1 - \beta$, power of the test, for example 90% $- \beta$, 10%; s, standard deviation, for example 0.6%ID g^{-1}; s_d, standard deviation of observed differences, for example 0.5%ID g^{-1}; d, relevant effect, for example 1% ID g^{-1}.
[c]Zielhuis (36).

3. CONCLUSION

We developed a dual-isotope SPECT protocol on a preclinial SPECT system and tested it for quantification of the biodistribution and tumor uptake of the angiogenesis tracer cRGD compared with its control cRAD. Single- and dual-isotope SPECT imaging as well as biodistribution data obtained with γ-counting showed tumor uptake of cRGD and no significant tumor uptake of cRAD. While having comparable organ uptake, it is concluded that cRAD is a valid nonspecific control for cRGD with respect to specific targeting of the $\alpha_v\beta_3$ receptor. Furthermore, the radionuclide used for radiolabeling of both peptides did not influence the biodistribution or binding affinity of the tracer. Using dual-isotope SPECT, the biodistribution of a nonspecific control can be quantified simultaneously with the specific tracer in the same animal. Provided that co-injection of both tracers does not affect their individual blood half-life and biodistribution, this approach provides an ideal internal reference and excludes any inter-animal variations and physiological changes, as well as reducing

Table 2. Summary of *in vivo* experiments

DOTA–cRGDfK	DOTA–cRADfK	Amount of peptide (nmol)	n[a]	Tumor-uptake (%ID cm^{-3})	Tumor-uptake (%ID g^{-1})
^{177}Lu		0.26	2	1.21 ± 0.28[b]	6.46 ± 1.86[b]
^{177}Lu		1.32	2	0.97 ± 0.19[b]	2.41 ± 0.56[b]
	^{177}Lu	0.26	2	0.11 ± 0.09[b]	0.17 ± 0.16[b]
	^{177}Lu	1.32	2	0.00 ± 0.00[b]	0.26 ± 0.01[b]
^{111}In		1.32	2	0.75 ± 0.14[b]	2.34 ± 2.09[b]
	^{111}In	1.32	2	0.08 ± 0.06[b]	0.41 ± 0.33[b]
^{177}Lu	^{111}In	1.32	5	1.54 ± 0.92[b]; 0.17 ± 0.08[b]	3.40 ± 0.47[b]; 0.18 ± 0.13[b]
^{111}In	^{177}Lu	1.32	4	1.50 ± 0.72[b]; 0.26 ± 0.05[b]	2.94 ± 0.31[b]; 0.24 ± 0.13[b]
^{177}Lu, ^{111}In		1.32	2	1.80 ± 0.44[b]; 1.58 ± 0.41[b]	2.54 ± 0.91[b]; 2.65 ± 1.21[b]

[a]n = number of animals
[b]value $\pm$ SD.

the amount of animals required. We recently showed the value of this dual-isotope approach in the design of matrix metalloproteinase tracers (8) and currently apply it in the development of new molecular imaging ligands.

4. EXPERIMENTAL

4.1. Dual-isotope optimalization

The ^{111}In/^{177}Lu combination was analyzed and optimized, measuring crosstalk severity and sensitivity for different energy window settings. All measurements were performed on a small animal SPECT/CT system (nanoSPECT/CT®, Bioscan, USA) equipped with four detector heads and converging nine-pinhole collimators (pinhole diameter, 1 mm; maximum resolution, 0.8 mm) (32,33).

The amount of initially measured crosstalk was minimized by optimizing the acquisition energy windows for both radionuclides. The crosstalk was quantified in form of a crosstalk factor, which was defined as:

$$\gamma_1' = \gamma_1 - A\gamma_2 \text{ and } \gamma_2' = \gamma_2 - B\gamma_1$$

with A and B being crosstalk factors from radionuclide γ_2 to radionuclide γ_1 and γ_1 to γ_2 respectively. The factors used for phantom studies were determined by placing a known amount of one radionuclide in the scanner (γ_2, approximately 20 MBq, >100 kcounts per projection in 120–360 s), and acquire the signal using the energy window settings for both radionuclides. The crosstalk factor (A) was defined as the ratio between the amount of counts measured in the window for radionuclide γ_1 and the amount of counts measured in the window of radionuclide γ_2. Besides overlap of the emission peaks, the crosstalk factors depend on the amount of Compton scattering. As Compton scattering and attenuation effects increase under *in vivo* conditions, the crosstalk factors were determined again in mice to allow *in vivo* studies.

The crosstalk factors measured for the ^{111}In/^{177}Lu settings that were optimal in sensitivity and minimized in crosstalk in both phantoms and *in vivo* are shown in Table 1. The first setting consisted of four separate energy windows: a 20% window around 171 keV (from 153.9–188.1 keV) and a 15% window around 245 keV (226.6–263.4 keV) for ^{111}In-acquisition, and two 20% windows around 113 keV (101.7–124.3 keV) and 208 keV (187.2–228.8 keV) for ^{177}Lu-acquistion. In the second acquisition setting, the ^{177}Lu energy window around 113 keV was removed since this window was highly affected by the ^{111}In signal. Furthermore, all windows were reduced in size to 10% around 171 keV (162.5–179.6 keV), 10% around 245 keV (232.8–257.3 keV) and 10% around 208 keV (197.6–218.4 keV). As expected, in the second acquisition setting, the sensitivity for both radionuclides was reduced compared with the first acquisition setting by 81% and 38% for ^{111}In and ^{177}Lu respectively. In order to compensate for the loss in sensitivity, the scan times were increased when using setting 2. The crosstalk remaining after adjusting the energy acquisition windows was partly removed using proprietary crosstalk removal software of the manufacturer (InVivoScope version 1.39, background clean function disabled, Bioscan, USA), which utilized the user-defined crosstalk factors to subtract counts originating from radionuclide γ_1 in the acquisition window of radionuclide γ_2 and vice versa.

The dual-isotope acquisition and crosstalk removal protocols were tested in phantoms by simultaneous scanning of four phantoms containing known amounts of mixed ^{111}In and ^{177}Lu [vial 1, 100% ^{111}In (~7.7 MBq); vial 2, 78% ^{111}In and 25% ^{177}Lu; vial 3, 75% ^{177}Lu and 25% ^{111}In; vial 4, 100% ^{177}Lu (~25.7 MBq), Supporting Information, figure 1]. The separate activities detected by SPECT were quantified before and after crosstalk removal. The quantification error was calculated for each setting. Based on these results, energy window setting 2 was considered favourable over energy window setting 1 and was therefore used during further experiments (Supporting Information, figure 2).

The dual-isotope protocol was tested *in vivo* in BALB/c nu/nu mice using free radionuclides as tracer. The biodistribution of ^{111}In and ^{177}Lu was measured separately in single-isotope SPECT studies and compared with the biodistribution measured with dual-isotope SPECT after co-injection. The radiopharmaceuticals were dissolved in physiological Tris(hydroxymethyl)aminomethane buffer (100 µl, pH 7.38) or in phosphate-buffered saline (100 µl) and injected into the tail vein. In case of the dual-isotope scans, the radionuclides were either pre-mixed and co-injected (100 µl) or administered with two separate injections (50 µl each) into the same tail vein. For ^{177}Lu-scans, approximately 40 MBq activity was injected as opposed to 10 MBq for ^{111}In-scans to compensate for the difference in γ-abundance. Animals were killed by cervical dislocation 3 h after injection and imaged post-mortem to have a direct comparison between imaging and biodistribution data at this time point.

After image reconstruction, VOIs were selected around selected organs and tissues using both SPECT and CT data. All VOIs were drawn in triplicate and averaged to minimize drawing variation. Detected counts in the VOIs were converted to Becquerel using a quantification factor that was calculated at the start of each study using a known amount of the radionuclide of interest. The biodistribution results from SPECT were expressed as percentage injected dose per volume (%ID cm^{-3}). After scanning, the animals were dissected and the radioactivity in blood, heart, lung, liver, spleen, left kidney, muscle and thigh bone was measured using a γ-counter (Wizard 1480, Perkin Elmer, The Netherlands) using the multiple isotope counting mode. Control experiments showed that the average deviation in dual-isotope ^{111}In/^{177}Lu counting from single-isotope ^{111}In or ^{177}Lu counting was <2% for both radionuclides. Radioactivity uptake in the tissues was calculated as percentage injected dose per gram of tissue (%ID g^{-1}). These values were compared with the radioactive uptake as quantified from SPECT imaging.

4.2. $\alpha_v\beta_3$ Targeting

4.2.1. *DOTA–peptide conjugation*

DOTA was conjugated to cRGDfK and cRADfK for radiolabeling. Acetyl-protected cRGDfK or cRADfK (2 mg, 2.6 µmol in 400 µl H_2O; Absinth Services B.V., The Netherlands) was deacetylated using hydroxylamine solution (1 M, 1.9 ml). After 30 min at room temperature, the deacetylated cRGDfK or cRADfK was combined with maleimido-mono-amide–DOTA solution (4 mg, 5.2 µmol in 2.7 ml H_2O; Macrocyclics, USA). The reaction mixture was shaken overnight at room temperature to form cRGDfK–DOTA or cRADfK–DOTA (Fig. 1b). The desired product was purified using preparative reversed-phase high-performance liquid chromatography (RP-HPLC) to a purity of >98%, freeze-dried and dissolved in Millipore-purified water.

4.2.2. Radiolabeling

An aliquot of cRGDfK–DOTA or cRADfK–DOTA solution (1.9 μl, 1.4 nmol) was added to $^{177}LuCl_3$ (100 MBq) or $^{111}InCl_3$ (50 MBq) in ammonium acetate buffer or sodium acetate buffer respectively (300 μl, 0.2 M, pH 5.5). The crude mixture was shaken at $T = 353$ K for 30 min before the reaction was quenched by adding 10 μl of a 10 mM EDTA solution. Typically, in these conditions approximately 80% labeling yield was obtained for both peptides with both radionuclides. The radiolabeled peptides were purified by solid-phase extraction on C_8 Sep-Pak cartridges (Waters, USA). The product was eluted in two 100 μl fractions of 30% ethanol in Millipore-purified water. The fractions were pooled and concentrated to 80 μl under a stream of nitrogen. Ammonium acetate buffer (0.25 M, pH 8.0) was added to adjust the pH to 7.2.

Both radiotracers solutions exhibited >95% radiochemical purity at the time of injection, as confirmed by radio-TLC and radio-HPLC. Radio-TLC was performed on ITLC-SG plates (Pall, USA) eluted in a 200 mM EDTA in physiological saline solution and analyzed on a phosphor imager (FLA-7000, Fujifilm, Japan). Under these conditions, ^{111}In-EDTA and ^{177}Lu-EDTA migrated with $R_f = 0.9$ while the radiolabeled peptides remained at the origin ($R_f = 0.0$). Radio-HPLC analysis was carried out on an Agilent 1100 system equipped with a UV detector and a radioactivity Gabi detector (Raytest, Germany). The analyte was loaded on a C_{18} column (Agilent, Eclipse XDB C_{18}, 150 × 4.6 mm, 5 μm particle size), which was eluted with a linear elution gradient of 5–40% (v/v) acetonitrile in water with 0.1% formic acid (1 ml min^{-1} for 11 min), starting with 3 min of 5% acetonitrile in water. Free radionuclide eluted from the column after 2.2 min, and radiolabeled cRGDfK–DOTA and cRADfK–DOTA after 9.5 min. The solutions injected in mice contained 1.32 nmol of one peptide for single-isotope experiments (100 μl) or 1.32 nmol of each peptide (100 μl in total) for dual-isotope experiments.

4.3. Animal model

The dual-isotope protocol was tested *in vivo* in normal BALB/c nu/nu mice. The specific $\alpha_v\beta_3$ targeting effect of cRGD was assessed and compared with the cRAD-peptide as the nonbinding control. cRGDfK–DOTA and cRADfK–DOTA were both radiolabeled with ^{111}In and ^{177}Lu achieving >95% radiochemical purity and subsequently injected into tumor-bearing mice. The tumor cell line U87MG was chosen to establish tumor xenografts in nude mice as this cell line is known to show significant overexpression of $\alpha_v\beta_3$-integrin receptors (34). Therefore, BALB/c nu/nu mice (male, 11–15 weeks old) were injected with approximately 5×10^6 U87MG cells (human, glioblastoma-astrocytoma, ATCC, Manassas, USA) in phosphate-buffered saline (100 μl) subcutaneously on the left or right flank. The mice were imaged when the tumor reached a size of approximately 40–60 mm^3.

The *in vivo* studies performed are listed in Table 2. Both peptides were labeled with both radionuclides to study possible effects of the respective radionuclide on tumor uptake and biodistribution. Two different peptide doses were assessed using ^{177}Lu as radiolabel during the single-isotope studies (0.26 and 1.32 nmol). For the single-isotope studies with ^{111}In and the dual-isotope studies with both ^{111}In and ^{177}Lu, 1.32 nmol peptide was used since this was the minimum dose required to obtain sufficiently high activity for SPECT imaging using ^{111}In as radiolabel. The optimal imaging time point was determined to be 1 h after injection based on dynamic scans of the tumor uptake of ^{177}Lu–DOTA–cRGDfK and ^{177}Lu–DOTA–cRADfK (Supporting Information, figure 3). During further experiments, mice were sacrificed at this time point and imaged post-mortem to have a direct comparison between imaging and biodistribution data at this time point.

After SPECT and γ-counting, the homogeneity of the activity-uptake in the tumor was assessed by autoradiography using a phosphor imaging system. Two tumors harvested from mice administered with ^{177}Lu–DOTA–cRGDfK were sliced (slice thickness ± 1 mm) and placed on a phosphor imaging plate for 2 h. The activity distribution was imaged with 100 μm resolution using the same phosphor imager as for the ITLC plates. All animal experiments were approved by the animal welfare committee of the Maastricht University (The Netherlands) and were performed according to the U.S. National Institutes of Health principles of laboratory animal care (35) and the Dutch national law 'Wet op de Dierproeven' (Std 1985, 336).

Acknowledgments

The authors acknowledge Caren van Kammen, Maastricht University for her animal handling expertise, Suzanne Kivits for analyzing SPECT and CT data and Monique Berben (Life Science Facilities, Philips Research) for her help with the biodistribution studies. The authors especially thank Raffa Rossin (Philips Research) for fruitful discussions.

REFERENCES

1. Weissleder R RB, Rehemtulla A, Gambhir SS. *Molecular Imaging Principles and Practice*. People's Medical Publishing House-USA: Shelton, 2010.
2. Blankenberg FG. Molecular imaging: The latest generation of contrast agents and tissue characterization techniques. J Cell Biochem 2003; 90(3): 443–453.
3. Berman DS, Kang X, Tamarappoo B, Wolak A, Hayes SW, Nakazato R, Thomson LE, Kite F, Cohen I, Slomka PJ, Einstein AJ, Friedman JD. Stress thallium-201/rest technetium-99 m sequential dual isotope high-speed myocardial perfusion imaging. JACC Cardiovasc Imag 2009; 2(3): 273–282.
4. Hsieh PC, Lee IH, Yeh TL, Chen KC, Huang HC, Chen PS, Yang YK, Yao WJ, Lu RB, Chiu NT. Distribution volume ratio of serotonin and dopamine transporters in euthymic patients with a history of major depression – a dual-isotope SPECT study. Psychiat Res 2010; 184(3): 157–161.
5. van der Bruggen W, Bleeker-Rovers CP, Boerman OC, Gotthardt M, Oyen WJ. PET and SPECT in osteomyelitis and prosthetic bone and joint infections: a systematic review. Semin Nucl Med 2010; 40(1): 3–15.
6. Heiba SI, Kolker D, Mocherla B, Kapoor K, Jiang M, Son H, Rangaswamy B, Kostakoglu L, Savitch I, DaCosta M, Machac J. The optimized evaluation of diabetic foot infection by dual isotope SPECT/CT imaging protocol. J Foot Ankle Surg 2010; 49(6): 529–536.
7. Melis M, de Swart J, de Visser M, Berndsen SC, Koelewijn S, Valkema R, Boerman OC, Krenning EP, de Jong M. Dynamic and static small-animal SPECT in rats for monitoring renal function after 177Lu-labeled Tyr3-octreotate radionuclide therapy. J Nucl Med 2010; 51(12): 1962–1968.
8. van Duijnhoven SM, Robillard MS, Nicolay K, Grull H. Tumor targeting of MMP-2/9 activatable cell-penetrating imaging probes is caused by tumor-independent activation. J Nucl Med; 52(2): 279–286.
9. Du Y, Frey EC. Quantitative evaluation of simultaneous reconstruction with model-based crosstalk compensation for 99mTc/123I dual-isotope simultaneous acquisition brain SPECT. Med Phys 2009; 36(6): 2021–2033.
10. Kao PF, Wey SP, Yang AS. Simultaneous 99mTc and 123I dual-isotope brain striatal phantom single photon emission computed tomography: validation of 99mTc-TRODAT-1 and 123I-IBZM

simultaneous dopamine system brain imaging. Kaohsiung J Med Sci 2009; 25(11): 601–607.
11. Sanchez-Crespo A, Petersson J, Nyren S, Mure M, Glenny RW, Thorell JO, Jacobsson H, Lindahl SG, Larsson SA. A novel quantitative dual-isotope method for simultaneous ventilation and perfusion lung SPET. Eur J Nucl Med Mol Imag 2002; 29(7): 863–875.
12. Kadrmas DJ, Frey EC, Tsui BM. Simultaneous technetium-99 m/thallium-201 SPECT imaging with model-based compensation for cross-contaminating effects. Phys Med Biol 1999; 44(7): 1843–1860.
13. Heo J, Wolmer I, Kegel J, Iskandrian AS. Sequential dual-isotope SPECT imaging with thallium-201 and technetium-99 m-sestamibi. J Nucl Med 1994; 35(4): 549–553.
14. Ceccarelli C, Bianchi F, Trippi D, Brozzi F, Di Martino F, Santini P, Elisei R, Pinchera A. Location of functioning metastases from differentiated thyroid carcinoma by simultaneous double isotope acquisition of I-131 whole body scan and bone scan. J Endocrinol Invest 2004; 27(9): 866–869.
15. Zhu X, Park MA, Gerbaudo VH, Moore SC. Quantitative simultaneous In-111/Tc-99 m planar imaging in a long-bone infection phantom. Phys Med Biol 2007; 52(24): 7353–7365.
16. Port M, Idee JM, Medina C, Robic C, Sabatou M, Corot C. Efficiency, thermodynamic and kinetic stability of marketed gadolinium chelates and their possible clinical consequences: a critical review. Biometals 2008; 21(4): 469–490.
17. Haubner R, Wester HJ, Reuning U, Senekowitsch-Schmidtke R, Diefenbach B, Kessler H, Stocklin G, Schwaiger M. Radiolabeled alpha(v)beta3 integrin antagonists: a new class of tracers for tumor targeting. J Nucl Med 1999; 40(6): 1061–1071.
18. Avraamides CJ, Garmy-Susini B, Varner JA. Integrins in angiogenesis and lymphangiogenesis. Nat Rev Cancer 2008; 8(8): 604–617.
19. Brooks PC, Clark RA, Cheresh DA. Requirement of vascular integrin alpha v beta 3 for angiogenesis. Science 1994; 264(5158): 569–571.
20. Haubner R, Wester HJ, Burkhart F, Senekowitsch-Schmidtke R, Weber W, Goodman SL, Kessler H, Schwaiger M. Glycosylated RGD-containing peptides: tracer for tumor targeting and angiogenesis imaging with improved biokinetics. J Nucl Med 2001; 42(2): 326–336.
21. Janssen M, Frielink C, Dijkgraaf I, Oyen W, Edwards DS, Liu S, Rajopadhye M, Massuger L, Corstens F, Boerman O. Improved tumor targeting of radiolabeled RGD peptides using rapid dose fractionation. Cancer Biother Radiopharm 2004; 19(4): 399–404.
22. Beer AJ, Niemeyer M, Carlsen J, Sarbia M, Nahrig J, Watzlowik P, Wester HJ, Harbeck N, Schwaiger M. Patterns of alphavbeta3 expression in primary and metastatic human breast cancer as shown by 18 F-Galacto-RGD PET. J Nucl Med 2008; 49(2): 255–259.
23. Ferl GZ, Dumont RA, Hildebrandt IJ, Armijo A, Haubner R, Reischl G, Su H, Weber WA, Huang SC. Derivation of a compartmental model for quantifying 64Cu-DOTA-RGD kinetics in tumor-bearing mice. J Nucl Med 2009; 50(2): 250–258.
24. Sugahara KN, Teesalu T, Karmali PP, Kotamraju VR, Agemy L, Girard OM, Hanahan D, Mattrey RF, Ruoslahti E. Tissue-penetrating delivery of compounds and nanoparticles into tumors. Cancer Cell 2009; 16(6): 510–520.
25. Kok RJ, Schraa AJ, Bos EJ, Moorlag HE, Asgeirsdottir SA, Everts M, Meijer DK, Molema G. Preparation and functional evaluation of RGD-modified proteins as alpha(v)beta(3) integrin directed therapeutics. Bioconjug Chem 2002; 13(1): 128–135.
26. Mulder WJ, Strijkers GJ, Habets JW, Bleeker EJ, van der Schaft DW, Storm G, Koning GA, Griffioen AW, Nicolay K. MR molecular imaging and fluorescence microscopy for identification of activated tumor endothelium using a bimodal lipidic nanoparticle. FASEB J 2005; 19 (14): 2008–2010.
27. Boyd M, Sorensen A, McCluskey AG, Mairs RJ. Radiation quality-dependent bystander effects elicited by targeted radionuclides. J Pharm Pharmacol 2008; 60(8): 951–958.
28. Proffitt RT, Williams LE, Presant CA, Tin GW, Uliana JA, Gamble RC, Baldeschwieler JD. Tumor-imaging potential of liposomes loaded with In-111-NTA: biodistribution in mice. J Nucl Med 1983; 24(1): 45–51.
29. Breeman WA, van der Wansem K, Bernard BF, van Gameren A, Erion JL, Visser TJ, Krenning EP, de Jong M. The addition of DTPA to [177Lu-DOTA0,Tyr3]octreotate prior to administration reduces rat skeleton uptake of radioactivity. Eur J Nucl Med Mol Imag 2003; 30(2): 312–315.
30. Dijkgraaf I, Kruijtzer JA, Frielink C, Corstens FH, Oyen WJ, Liskamp RM, Boerman OC. Alpha v beta 3 integrin-targeting of intraperitoneally growing tumors with a radiolabeled RGD peptide. Int J Cancer 2007; 120(3): 605–610.
31. Antunes P, Ginj M, Zhang H, Waser B, Baum RP, Reubi JC, Maecke H. Are radiogallium-labelled DOTA-conjugated somatostatin analogues superior to those labelled with other radiometals? Eur J Nucl Med Mol Imag 2007; 34(7): 982–993.
32. Schramm NU, Lackas C, Forrer F, de Jong M, Hoppin JW, Van Cauter SC, Haemisch Y. The NanoSPECT/CT: a high-sensitivity small-animal SPECT/CT with sub-millimeter spatial resolution. Available from: http://appnotes.spect-ct.com/AppNote-011-High_Sensitivity_Small_Animal_SPECT-CT.pdf
33. Schramm NU, Hoppin JW, Lackas C, Gershman B, Norenberg JP, de Jong M. The NanoSPECT/CT: a high-performance SPECT/CT for small-animal research. Available from: http://appnotes.spect-ct.com/AppNote-012-High-Perf_SPECT-CT_for_Small-Animals.pdf
34. Zhang X, Xiong Z, Wu Y, Cai W, Tseng JR, Gambhir SS, Chen X. Quantitative PET imaging of tumor integrin alphavbeta3 expression with 18 F-FRGD2. J Nucl Med 2006; 47(1): 113–121.
35. NIH. *Guide for the Use and Care of Laboratory Animals*, Vol. 86. National Academy Press: Washington, DC; 1985.
36. Zielhuis GA. *Handleiding medisch-wetenschappelijk onderzoek*. Elsevier Gezondheidszorg: Maarssen, 2000; 87–98.